Enhanced bipolar resistive switching behavior in polar Cr-doped barium titanate thin films without electro-forming process

Atul Thakre, and Ashok Kumar

Citation: AIP Advances **7**, 125115 (2017); doi: 10.1063/1.5004232
View online: https://doi.org/10.1063/1.5004232
View Table of Contents: http://aip.scitation.org/toc/adv/7/12
Published by the American Institute of Physics

Enhanced bipolar resistive switching behavior in polar Cr-doped barium titanate thin films without electro-forming process

Atul Thakre[1,2] and Ashok Kumar[1,2,a]
[1]CSIR-National Physical Laboratory, Dr. K. S. Krishnan Marg, New Delhi 110012, India
[2]Academy of Scientific and Innovative Research (AcSIR), CSIR-National Physical Laboratory (CSIR-NPL) Campus, Dr. K. S. Krishnan Road, New Delhi 110012, India

(Received 12 September 2017; accepted 2 December 2017; published online 14 December 2017)

An enhanced, repeatable and robust resistive switching phenomenon was observed in Cr substituted $BaTiO_3$ polar ferroelectric thin films; fabricated and deposited by the sol-gel approach and spin coating technique, respectively. An enhanced bistable bipolar resistive switching (BRS) phenomenon without electro-forming process, low switching voltage (~ 2 V) and moderate retention characteristics of 10^4 s along with a high R_{off}/R_{on} resistance ratio ~10^3 was achieved. The current conduction analysis showed that the space charge limited conduction (SCLC) and Schottky emission conduction dominate in the high voltage range, while thermally active charge carriers (ohmic) in the lower voltage range. The impedance spectroscopy study indicates the formation of current conducting path and rupturing of oxygen vacancies during SET and RESET process. https://doi.org/10.1063/1.5004232

Information technology world becomes incredibly demanding from last two decades since conventional charge-based memories are approaching its saturation due to its scaling limits.[1] The alternate memory architectures such as ferroelectrics random access memory (FeRAM), magnetic random access memory (MRAM) and phase change random access memory (PRAM), etc. have been proposed by various scientific groups.[2–4] Among nonvolatile random access memory (NVRAM) elements, resistive switching random access memory (ReRAM) has proven itself a promising candidate for future generation technology due to its superior features like high scaling, very simple structure, low power consumption, high resistance ratio, long data retention, high density, high switching speed and compatibility with the complementary metal oxide semiconductor (CMOS) memory technology.[5–7] Resistive switching (RS) phenomenon is based on a simple principle of applied electric field stimulated switching of the two (multiple in case of Memristors[8]) resistive states, i.e., from high resistance state (HRS) to low resistance state (LRS) or vice versa. The switching from HRS to LRS is termed as SET or WRITE process whereas LRS to HRS is termed as RESET or ERASE process. Categorically, the RS phenomenon can be divided into Unipolar or non-polar resistive switching (URS) and bipolar resistive switching (BRS) according to the polarity of SET and RESET external electric field. In URS, SET and RESET processes occur on the same side of the applied electric field's polarity (either in positive or negative) whereas BRS has the SET and RESET processes on the different side of the polarity. In comparison, BRS provides more uniformity, higher resistivity, and lower switching voltage whereas URS has higher ON/OFF ratio of resistance states.[9] In quest of future generation ReRAM memory, several materials such as polymers,[10–13] carbon-based materials,[14,15] rare earth oxides,[16–18] various perovskite-type oxides structures[19,20] and transitional metal oxides[21,22] etc. are being studied. Among the various perovskite type oxide materials, barium titanate (BTO) is a very popular and has been extensively studied because of its some unique features such as the presence of

[a]Corresponding Author: Dr. Ashok Kumar (ashok553@nplindia.org)

spontaneous polarization, high dielectric permittivity, high electro-optic coefficient and good compatibility with the existing conventional semiconductor technology.[6,23–25] In the recent time, some of the researchers have reported the RS phenomenon, diode characteristics, and large hysteresis in the current-voltage graph in BTO or transition metal doped BTO thin films.[26–30] Li et al[31] and Chang et al[28] reported the BRS behavior in the multilayer BTO thin film with a very high compliance current ~ 100 mA. Similarly, Yan et al[32] reported URS behavior in the Co doped BTO thin films with a compliance current ~ 100 mA. In addition, Chang et al. reported an ON/OFF ratio study with varying top electrodes such as Al, ITO, Au and Pt; where it shows that Au and Pt as top metal electrodes offer the R_{off}/R_{on} ratio ~10. Recently Jin et al[30] reported BRS behavior in Nb doped BTO thin films with large current density ~10^3 A/cm^2. We present the BRS behavior without electro-forming process and maximum current density of 1 A/cm^2 with a resistance ratio of ~1000 when top electrode is Au. As per the best of our knowledge, no sharp-switching of resistance from HRS to LRS and vice versa with a very low compliance current has been reported so far on BTO or doped BTO thin film systems.

In this report, we present the BRS phenomenon in Au/CrBTO/ITO thin film memory device without electro-forming process and R_{off}/R_{on} ratio of 10^3 by substitution of mixed valance Cr^{3+}/Cr^{5+} on Ti^{4+} site. The optimized 10% Cr doped $BaTiO_3$ (CrBTO) thin films were fabricated by the Sol-Gel method. The CrBTO provides an extra degree of freedom due to the presence of spontaneous polarization. A robust and repeatable BRS behavior has been presented for Au/CrBTO/ITO crossbar structure deposited by a spin-coating method. The impedance spectra, charge retention, and endurance quality has been described regarding LRS and HRS.

The synthesis of CrBTO solution for the thin film deposition was prepared by Sol-Gel method. Barium Acetate ($(CH_3COO)_2$ Ba), Titanium IV isopropoxide (Ti [OCH $(CH_3)_2]_4$) and Chromium Acetate ($Cr(CH_3COO)_3$) were used as precursors. In the preparation of the solution, Acetic acid (CH_3COOH) and 2-methoxy ethanol ($C_3H_8O_2$) were also used as solvents. At first, a solution (say 'A') of acetic acid and 2-methoxy ethanol was prepared to have 1:1 ratio. In the solution 'A', a calculated amount of ethylene glycol was mixed and kept for stirring for 10 min. After this, an appropriate amount of barium acetate was dissolved in Sol 'A' and kept for stirring with 50^0C heating till it fully dissolves and forms a transparent solution (say solution 'B'). After this, a calculated amount of Titanium IV isopropoxide (TIP) and Chromium Acetate were added simultaneously into the solution 'B'. The ratio of Titanium IV isopropoxide and Chromium Acetate was kept 9:1 to make 10 mol% Cr-doped BTO solutions. Here TIP was added drop by drop by micropipette into the stirring solution to prevent any pre-precipitation of TIP. The prepared solution was then kept in a closed flask and stirred for 5 hrs. The ITO-coated glass was used as substrates for film deposition. The substrates were cleaned with IPA and Acetone with 2 min sonication process. The CrBTO thin films were prepared by the spin-coating technique. For the deposition of the thin films, spin coater model NXGM1 was used, and thin films were prepared at 3500 rpm for 30 sec. The prepared thin films were first dried at 250 ^{0}C on a hot plate for one hr to remove the organics and then annealed at 700^0C for one hr. Later, for the electrical measurements, a capacitive structure was formed. The top electrode of Au having circular patterning with a diameter of 200 μm was sputtered through a shadow mask. The RS measurements, impedance spectroscopy, and polarization-electric field measurements were performed using Keithley 236 source-meter, Hioki 3532-50 LCR HiTester, and a Precision Multiferroic tester (Radiant Technologies Inc.), respectively. These electrical and dielectric measurements were carried out using a micro-probe system at room temperature. The surface topography was characterized by Atomic Force Microscopy (AFM) and data were analyzed by Gwyddion software. The CrBTO thin films crystalline phases and film thickness were characterized by X-ray diffraction technique and profilometer.

The crystalline phases of the annealed CrBTO thin films along with the bare ITO coated glass substrate were characterized by X-Ray diffraction technique as shown in Fig 1(a). The diffraction peaks at 31.5^0 and 31.6^0 corresponded to (110) and (110) planes,[33] respectively. The weak diffraction patterns of CrBTO are shown in the inset of Fig 1(a) which may be due to a nanoscale thickness of films which was hard to detect by powder XRD machine. Fig 1(b) depicts the AFM image of the top surface of Au/CrBTO/ITO RS device. The average thickness and roughness of the CrBTO thin film

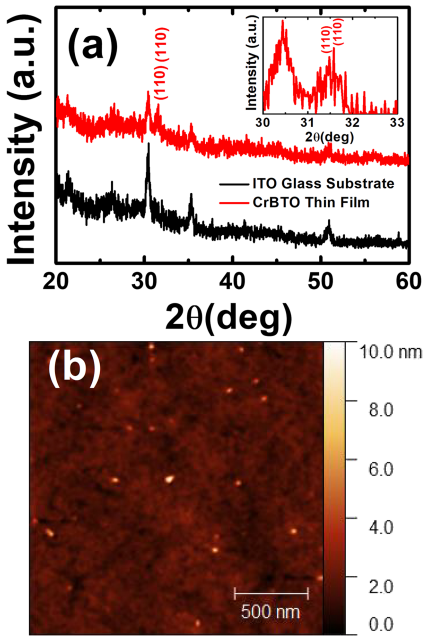

FIG. 1. (a) shows the XRD plot of the ITO coated glass substrate and CrBTO thin film deposited over the ITO glass substrate and inset plot shows the peaks at 31.5^0 and 31.6^0 of the CrBTO thin film; and (b) AFM image of the top surface of the CrBTO thin film.

were found 50 (+/- 5) nm and 1-2 nm depending on probe area, in general films top surface was quite smooth.

In Fig 2(a), the semi-log plot of current-voltage characteristics and forming free bipolar resistive switching behavior of Au/CrBTO/ITO at room temperature has been shown. The inset image in Fig 2(a) depicts the schematic device structure. In the current-voltage measurement, a voltage sweep

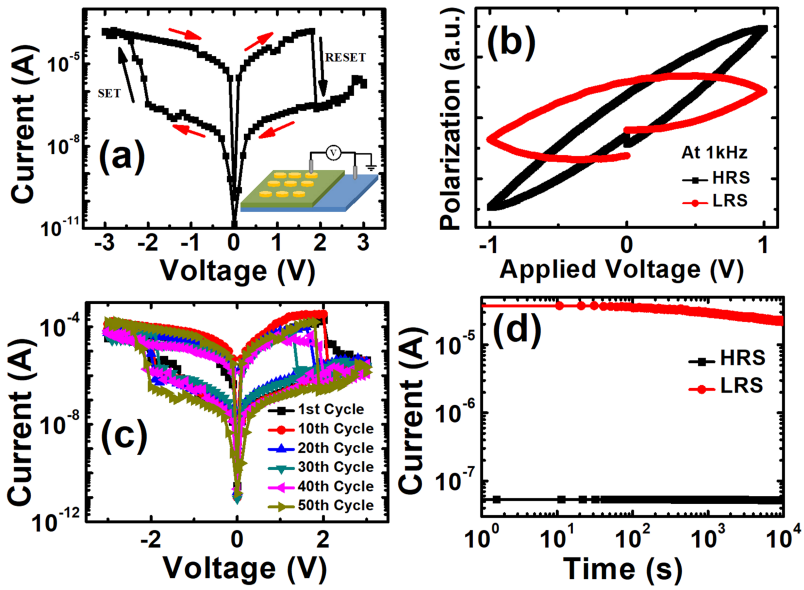

FIG. 2. (a) indicates I-V plot of the Au/CrBTO/ITO memory device which demonstrates the BRS behaviour. The inset image depicts the schematic of the device structure; (b) The P-E plots of the device for HRS (Black) and LRS (Red and lossy shape). (c) The endurance characteristics plot for the 50 consecutive successful cycles; (d) The retention properties of the device for 10^4 s.

of -3V→3V→-3V was applied on top Au electrode while keeping the bottom ITO electrode grounded. To prevent the devices from the permanent dielectric breakdown, a compliance current of 1 mA was fixed for SET and RESET process. However, devices never achieved such high compliance values. Initially, when applied voltage sweep starts from -3V, the pristine device showed the LRS state till the applied voltage sweep approaches to 2V, the current passing through the device abruptly decreases by a large ratio; i.e., RESET phenomena occurred. Upon continuation, when the voltage-sweep approaches from 3V to -3V, the current through the device increase abruptly nearly -2V; i.e., near the SET voltage. The maximum current passing through the device was in the range of ~100 μA, which is acceptable for the device application. Fig 2(c) and (d) show that the device exhibited excellent endurance characteristics for 50 consecutive stress cycles and the retention characteristics up to 10^4 s, respectively. For clarity, RS plot after every ten cycles has been shown in Fig. 2(c). The retention characteristics were recorded at a constant bias voltage of 0.5V for both resistive states which show almost constant current over a large period. A slight reduction of nearly 15 μA in the current values was observed over a period of 10^4 s, however, with further continuing the retention test for 10^8 s, the decrement settled with a resistance ratio of ~500. To investigate the ferroelectric phase of the CrBTO, polarization-electric field (P-E) characteristics have been performed for the low applied electric field (less than the SET and RESET voltage) at 1 kHz after SET and RESET processes which indicate a slim hysteresis in HRS whereas a leaky round shape P-E loops in LRS, as shown in Fig. 2(b). The P-E data suggests the presence of spontaneous polarization in CrBTO films which played an important role in the sharp change in resistance states. During RESET process, the polarization and positive bias at top Au electrode depleted the presence of oxygen vacancies near electrode which discontinued the conduction path and hence change in resistance states.

To investigate the dominating conduction mechanism in the resistive switching phenomena, *I-V* plot was replotted as log-log scale, and respective slopes were obtained from the linear fitting, as shown in Fig 3(a). The space charge limited conduction (SCLC)[34,35] mechanism was investigated for the resistive switching device, and *log J vs. log E* plot was well fitted to a straight line. The current density and applied electric field relationship in SCLC conduction mechanism can be expressed as below,

$$J_{SCLC} = (9/8)\,\mu\varepsilon\theta E^2/d. \tag{1}$$

where J_{SCLC} is the current density in the SCLC mechanism, μ is the mobility of charge carriers, ε is the static dielectric constant, θ is the ratio of injected charge carriers to the total charge carriers, E is the applied electric field and d is the thickness of the dielectric thin film. From the linear fitting of the *log-log* plot, the obtained slope in the LRS for the low applied electric field (between ~ 6 to 7 V/m) is ~1, indicating ohmic conduction in the LRS. Whereas on further increment in the applied field, the slope slightly increases to ~ 1.26; indicating more charge carriers are contributing into the conduction. Similarly, in the HRS the slope was ~1.4 which indicates the dominant trap-assisted SCLC conduction mechanism.

The aforementioned increment in the slope in the LRS leads to investigate the Schottky conduction mechanism.[36] The current-voltage plot was re-plotted as *ln J vs.* $E^{1/2}$ and linearly fitted as shown in Fig 3(b). The relationship between the current density and applied electric field in Schottky emission conduction is given below,

$$J = A^* T^2 exp\left[\frac{-q\left(\emptyset_B - \sqrt{qE/4\pi\varepsilon_0\varepsilon_r}\right)}{kT}\right]. \tag{2}$$

where J is current density, A^* is effective Richardson constant, T is absolute temperature, q is electronic charge, $q\Phi_B$ is Schottky barrier height, E is the applied electric field across the thin film device, ε_0 and ε_r are absolute and optical dielectric constant, respectively, and k_B is the Boltzmann's constant. In the applied voltage sweep of -3V to 0V, for the higher electric field region (nearly from 3 kV/m to 5.5 kV/m) in the LRS, the obtained slope value (~0.0006) from linear fitting of the *ln J vs.* $E^{1/2}$ plot yielded an optical dielectric constant very close to that of barium titanate (ε~5.76) which clearly demonstrates the domination of Schottky emission in the conduction process in LRS. Thus, the RS phenomenon in the CrBTO memory device and the higher current in the LRS can be attributable

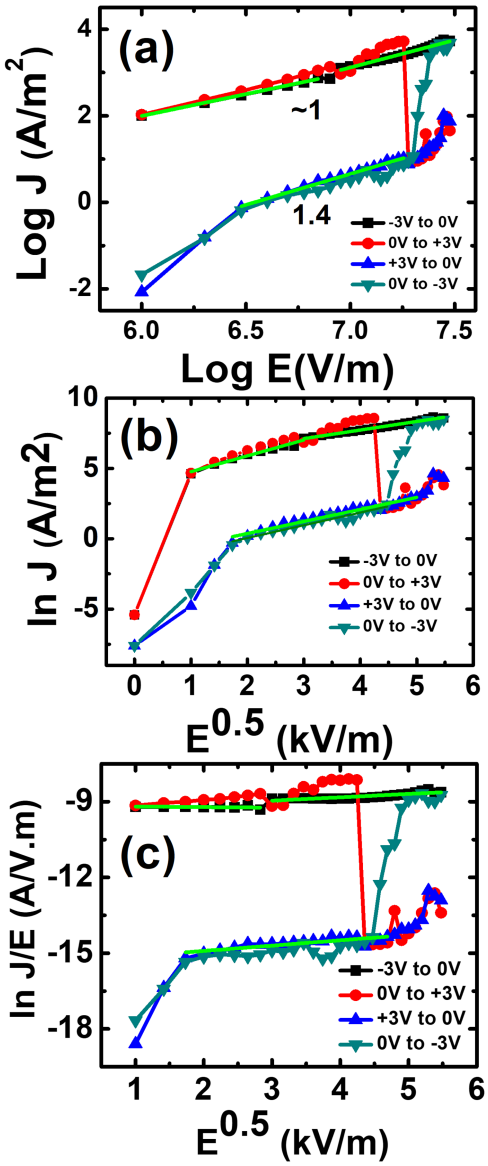

FIG. 3. The current conduction behavior and its fitting (solid line) with various conduction models i.e., (a) SCLC, (b) Schottky emission, and (c) Pool-Frankel, respectively.

to the modulation of the Schottky barrier height because of the oxygen vacancies migration. In this investigation, the Schottky barrier height is also calculated for the higher applied electric field region (from 3 kV/m to 5.5 kV/m) in the LRS, from the Eq. 2. In this region, the obtained value of the Schottky barrier height was ~0.32 eV; which demonstrating the modulation of the Schottky barrier height in the LRS region. Similarly, for the Poole-Frankel emission investigation, shown in the Fig 3(c), slopes from the linear fitting of the *ln (J/E) vs.* $E^{1/2}$ plot, yielded unrealistic optical dielectric constant of the Cr-doped BTO thin film that ruled out the possibilities of Poole-Frankel emission conduction mechanism. The energy band diagram for the Au/CrBTO/ITO device has been shown in the Fig. 5(c). Here, the work function of the top Au electrode and bottom ITO electrode is 5.1 eV and 4.5 eV.[37] The electron affinity and energy band gap of the CrBTO is used as 3.8 eV and 3.4 eV, respectively[38] which are obtained from earlier reports. On the pristine device, the potential barrier height is ~1.3 eV. When the voltage sweep starts from 0V to -3V, oxygen vacancies are pulled up towards the top Au electrode, which eventually lowers down the Schottky barrier height to 0.325 eV;

TABLE I. A comparative study on various parameters of RS memory devices and elements with respect to other available similar device structures in literature.

S.N.	Device Structure	Synthesis Method	Current compliance	R_{off}/R_{on} Ratio	Retention Time	Endurance	Ref.
1.	Au/Co:BTO/Pt	Sol-Gel	~100 mA	$\sim 10^6$	-	-	31
2.	Al/BTO/ITO	Sol-Gel	~100 mA	$\sim 10^6$	10^5 s	-	28
3.	Au/Co:BTO/Pt	PLD	~10 mA	$\sim 10^4$	10^4 s	10^5 Cycles	32
4.	Au/Cr:BTO/ITO	Sol-Gel	~100 μA	$\sim 10^3$	10^4 s	50 Cycles	present

thus conducting paths of the oxygen vacancies were formed and the device enters into the LRS. Similarly, as the voltage sweep further approaches from 0V to 3V, the oxygen vacancies are pushed down towards the bottom ITO electrode; which ruptures the conducting path and results in the RESET process. A comparative study of the resistive switching parameters of the proposed system with the other reported BTO or doped BTO systems has been given in Table I.

To further thoroughly analyze the conduction mechanism, impedance spectroscopy measurements were performed. Various frequency dependent parameters such as impedance, phase angle, capacitance, and tangent loss have been recorded for the frequency range of 100 Hz to 1 MHz. Frequency-dependent impedance plots (Fig. 4(a & c)) and their respective Nyquist plot (Fig. 4(b & d)) with equivalent electrical circuit fitting in LRS and HRS have been shown in Fig. 4(a–d). Fig. 4(b) and 4(d) show a large impedance difference in LRS (kΩ) and the HRS (MΩ). It can also be observed that the relaxation time decreases by a large ratio (μs to s) in RESET process; which explains the damping rate of hopping of charge carriers which results in the HRS.[39] The Nyquist plot was fitted with an equivalent electrical circuit comprising a R_s (contact resistance) connected in the series with a parallel combination of R_{bulk} (bulk resistance) and C_{bulk} (bulk capacitance). From the fitted plots, the obtained parameters show that in the SET process, R_s (contact resistance of electrode-dielectric) changes from 1200 Ω to 700 Ω and R_{bulk} (dielectric resistance) changes drastically from ~5.6 MΩ to ~1 kΩ. Thus, it is asserting that the RS phenomenon is driven by the large change in bulk resistance due to the formation of conducting oxygen vacancies path inside the CrBTO thin film. Fig 5(a) and (b) exhibit the frequency dependency behavior of capacitance and tangent loss of the CrBTO thin films. It can be seen that the capacitance is almost same in both resistive states; LRS and HRS. A negligible change in the capacitance and an order change

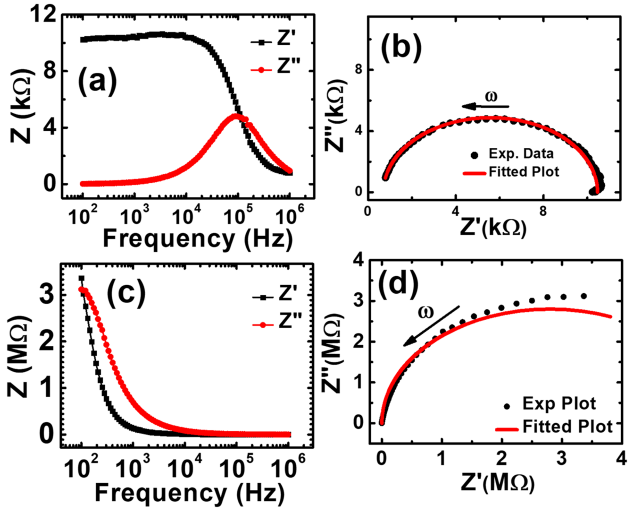

FIG. 4. (a) and (c) show the frequency dependence of the real and imaginary impedance data of the Au/CrBTO/ITO device in LRS and HRS, respectively; (b) and (d) show the Nyquist plots for the LRS and HRS, respectively with an equivalent electrical circuit (solid line).

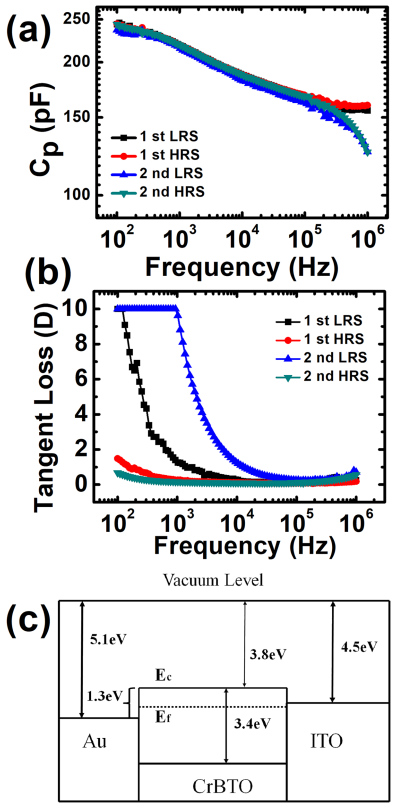

FIG. 5. (a) and (b) show the frequency dependence of the capacitance and tangent loss data, respectively, and (c) Energy band diagram of the Au/CrBTO/ITO capacitive device.

in a tangent loss during SET processes support the development of several parallels conducting paths. These results favor the formation of several capacitors connected in parallel and separated by conducting path which in turns provides almost similar capacitance and an order change in the tangent loss.

In summary, we fabricated a crossbar Au/CrBTO/ITO memory device for resistive switching effects. Ultra thin films of non-polar oxides show RS effect with the noble metal and conducting oxide electrodes. Ferroelectrics are highly resistive (> GΩ) in nature, we introduced a controlled amount of Cr into the BTO matrix to make it more conductive and possible candidate for resistive switching. We found a robust and sharp bipolar resistance switching in CrBTO at a very low applied electric field and without reaching to the electro-forming process. The sharp BRS phenomenon can be explained by the migration of oxygen vacancies and active role of polarization under various bias electric field which eventually forming several parallel conducting paths during SET process.

[1] J. F. Scott, Annu. Rev. Mater. Sci. **28**, 79 (1998).
[2] Y. A. Hiroshi Ishiwara and M. Okuyama, *Ferroelectric Random Access Memories: Fundamentals and Applications* (Springer, 2004).
[3] R. C. Sousa and I. L. Prejbeanu, Comptes Rendus Phys. **6**, 1013 (2005).
[4] T.-C. Chang, K.-C. Chang, T.-M. Tsai, T.-J. Chu, and S. M. Sze, Mater. Today **19**, 254 (2016).
[5] R. Waser and M. Aono, Nat. Mater. **6**, 833 (2007).
[6] R. Waser, R. Dittmann, C. Staikov, and K. Szot, Adv. Mater. **21**, 2632 (2009).
[7] H. Akinaga and H. Shima, Proc. IEEE **98**, 2237 (2010).
[8] D. B. Strukov, G. S. Snider, D. R. Stewart, and R. S. Williams, Nature **453**, 80 (2008).
[9] F. C. Chiu, Adv. Mater. Sci. Eng. **2014**, 1.
[10] S. R. Mohapatra, T. Tsuruoka, T. Hasegawa, K. Terabe, and M. Aono, AIP Adv. **2**, 22144 (2012).
[11] G. Khurana, P. Misra, and R. S. Katiyar, Carbon N. Y. **76**, 341 (2014).
[12] A. Thakre, H. Borkar, B. P. Singh, and A. Kumar, RSC Adv. **5**, 57406 (2015).
[13] A. Thakre and A. Kumar, J. Alloys Compd. **722**, 579 (2017).

[14] H. Y. Jeong, J. Y. Kim, J. W. Kim, J. O. Hwang, J. E. Kim, J. Y. Lee, T. H. Yoon, B. J. Cho, S. O. Kim, R. S. Ruoff, and S. Y. Choi, Nano Lett **10**, 4381 (2010).
[15] G. Liu, X. Zhuang, Y. Chen, B. Zhang, J. Zhu, C. X. Zhu, K. G. Neoh, and E. T. Kang, Appl. Phys. Lett. **95**, 253301 (2009).
[16] X. Cao, X. Li, X. Gao, W. Yu, X. Liu, Y. Zhang, L. Chen, and X. Cheng, J. Appl. Phys. **106**, 073723 (2009).
[17] Y. Cui, H. Peng, S. Wu, R. Wang, and T. Wu, ACS Appl. Mater. Interfaces **5**, 1213 (2013).
[18] F. Pan, S. Gao, C. Chen, C. Song, and F. Zeng, Mater. Sci. Eng. R Reports **83**, 1 (2014).
[19] H. Nili, S. Walia, S. Balendhran, D. B. Strukov, M. Bhaskaran, and S. Sriram, Adv. Funct. Mater. **24**, 6741 (2014).
[20] Z. B. Yan and J. M. Liu, Ann. Phys. (N. Y). **358**, 206 (2015).
[21] D. Panda and T.-Y. Tseng, Ferroelectrics **471**, 23 (2014).
[22] A. Sawa, Mater. Today **11**, 28 (2008).
[23] M. J. Dicken, L. A. Sweatlock, D. Pacifici, H. J. Lezec, K. Bhattacharya, and H. A. Atwater, Nano Lett. **8**, 4048 (2008).
[24] S. Zafar, R. E. Jones, B. Jiang, B. White, V. Kaushik, and S. Gillespie, Appl. Phys. Lett. **73**, 3533 (1998).
[25] L. Huang, Z. Chen, J. D. Wilson, S. Banerjee, R. D. Robinson, I. P. Herman, R. Laibowitz, and S. O'Brien, J. Appl. Phys. **100**, 34316 (2006).
[26] D. S. Jeong, R. Thomas, R. S. Katiyar, J. F. Scott, H. Kohlstedt, A. Petraru, and C. S. Hwang, Reports Prog. Phys. **75**, 76502 (2012).
[27] A. Visinoiu, R. Scholz, M. Alexe, and D. Hesse, Appl. Phys. A **80**, 229 (2005).
[28] Y.-C. Chang, R.-Y. Xue, and Y.-H. Wang, IEEE Trans. Electron Devices **61**, 4090 (2014).
[29] Y. Heo, D. Kan, Y. Shimakawa, and J. Seidel, Phys. Chem. Chem. Phys. **18**, 197 (2016).
[30] Q. Jin, C. Zheng, Y. Zhang, C. Lu, J. Dai, and Z. Wen, Appl. Phys. Lett. **111**, 1 (2017).
[31] S. Li, H. Z. Zeng, S. Y. Zhang, and X. H. Wei, Appl. Phys. Lett. **102**, 153506 (2013).
[32] Z. Yan, Y. Guo, G. Zhang, and J. M. Liu, Adv. Mater. **23**, 1351 (2011).
[33] J. P. B. Silva, F. L. Faita, K. Kamakshi, K. C. Sekhar, J. A. Moreira, A. Almeida, M. Pereira, A. A. Pasa, and M. J. M. Gomes, Sci. Rep. **7**, 1 (2017).
[34] A. Rose, Phys. Rev. **97**, 1538 (1955).
[35] A. A. Grinberg, S. Luryi, M. R. Pinto, and N. L. Schryer, IEEE Trans. Electron Devices **36**, 1162 (1989).
[36] P. R. Emtage and W. Tantraporn, Phys. Rev. Lett. **8**, 267 (1962).
[37] J. P. B. Silva, F. L. Faita, K. Kamakshi, K. C. Sekhar, and J. A. Moreira, Nat. Publ. Gr. **7**, 1 (2017).
[38] S. Y. Wang, M. Li, W. F. Liu, and J. Gao, Phys. Lett. Sect. A Gen. At. Solid State Phys. **379**, 1288 (2015).
[39] E. Barsoukov and J. R. Macdonald, *Impedance Spectroscopy* (2005).